

## Bulk and surface electronic structures of CePdX ( $X=As,Sb$ ) studied by 3d-4f resonance photoemission

T. Iwasaki, S. Suga, S. Imada, A. Sekiyama, K. Matsuda, M. Kotsugi, K.-S. An,\* T. Muro,† S. Ueda, and T. Matsushita‡

*Department of Material Physics, Faculty of Engineering Science, Osaka University, Toyonaka, Osaka 560-8531, Japan*

Y. Saitoh and T. Nakatani

*Japan Atomic Energy Research Institute, SPring-8, Mikazuki, Hyogo 679-5198, Japan*

H. Ishii and O. Sakai

*Department of Physics, Tokyo Metropolitan University, Hachioji, Tokyo 192-0397, Japan*

R. Takayama‡ and T. Suzuki

*Department of Physics, Tohoku University, Sendai 980-8578, Japan*

T. Oguchi

*Department of Physics, Hiroshima University, Higashi-Hiroshima 739-8526, Japan*

K. Katoh

*Department of Mathematics and Physics, The National Defense Academy, Yokosuka 239-8686, Japan*

A. Ochiai

*Department of Material Science and Technology, Niigata University, Niigata 950-2181, Japan*

(Received 8 September 1999)

We have performed Ce 3d-4f resonance photoemission spectroscopy (RPES) for CePdAs and CePdSb and compared the results with those of Ce 4d-4f RPES. The 3d-4f RPES spectra are remarkably different from the 4d-4f RPES spectra, showing the smaller contribution of the surface electronic structures in the 3d-4f RPES. On the other hand, the 3d-4f and 4d-4f resonance-minimum spectra for CePdSb are well described by the band-structure calculations for LaPdSb by taking the photoionization cross sections into account. This indicates that the surface effect is negligible in the resonance-minimum spectra. The theoretical calculation based on the single-impurity Anderson model well reproduces the surface- and bulk-sensitive Ce 4f spectra of both compounds, revealing that the difference between the surface and bulk electronic states originates mainly from the surface core-level shift of the bare 4f level. The spectral difference between the two compounds is explained by the different energy dependence of the hybridization strength.

### I. INTRODUCTION

Many cerium compounds have been extensively studied by various experimental and theoretical methods because of their fascinating physical properties, for example, the Kondo effect, heavy-fermion phenomena, and valence fluctuation. They originate from peculiar behaviors of strongly correlated Ce 4f electrons near the Fermi level ( $E_F$ ). The Ce 4f electrons show itinerant characters through the hybridization between the Ce 4f and other valence electron states. In order to probe the Ce 4f electron states, photoemission spectroscopy is a very useful method.<sup>1</sup> In particular, resonance photoemission spectroscopy (RPES) using synchrotron radiation is very effective in revealing the electronic states such as Ce 4f orbit.<sup>2</sup> A widely used Ce 4d-4f RPES has an advantage of good energy resolution, which enables one to observe such fine structures as the Ce 4f spin-orbit splitting of the order of 300 meV.<sup>3,4</sup> However, the small mean free path of the photoelectron is a weak point of the 4d-4f RPES for probing bulk electronic states. On the other hand, Ce 3d-4f RPES measurements provide relatively bulk-sensitive information

of electronic states. It has been reported that the Ce 3d-4f RPES spectra show Ce 4f spectral line shapes remarkably different from those of the 4d-4f RPES,<sup>5-11</sup> indicating that the Ce 4d-4f RPES spectra strongly reflect contributions from the surface region due to the shorter mean-free path of the excited electron. However, the energy resolution of the 3d-4f RPES has so far been not sufficient to resolve such fine structures near  $E_F$ , making it difficult to quantitatively discuss the difference between the surface and bulk electronic states. Very recent development in high brilliance synchrotron radiation source and instrumentation enable us to do the high-energy excitation RPES with sufficient energy resolution. Thus we can compare the details of the bulk-sensitive 3d-4f RPES results with the surface-sensitive 4d-4f RPES spectra.

CePdAs and CePdSb are two dimensional layered compounds, which are composed of the Ce layer and the Pd-X layer piled up along the  $c$  axis. The crystal structure of CePdAs is the hexagonal ZrBeSi type with the Pd and As atoms in a plane while CePdSb has the hexagonal LiGaGe-type crystal structure, where the Pd and Sb atoms form puckered

layers.<sup>12–14</sup> The distance between the nearest neighbor Ce atoms in the  $c$  plane is larger than that along the  $c$  axis in both compounds, suggesting that the hybridization of the Ce  $4f$  states may be much weaker within the  $c$  plane. According to the previous Ce  $3d$  x-ray photoemission spectroscopy study,<sup>15</sup> these compounds show nearly trivalent character and are understood to be weakly hybridized systems. CePdAs is antiferromagnetic below around  $T_N=4$  K with an anisotropy with respect to the  $c$  axis in the electric resistivity and the magnetic susceptibility. The magnetic moments of the Ce atoms lie in the  $c$  plane and antiferromagnetically ordered along the  $c$  axis in the ground states.<sup>12</sup> On the other hand, CePdSb has a ferromagnetic ground state with the easy magnetization axis in the  $c$  plane.<sup>12</sup> Its magnetic ordering is characterized by a rather high Curie temperature  $T_C=17.5$  K in contrast to other Ce compounds and other isostructural RPdSb compounds ( $R=\text{Nd, Sm, Eu, Gd}$ ), which order antiferromagnetically.<sup>13</sup>

Ce pnictide compounds are well-known to show various unusual properties derived from the peculiar electronic structures near  $E_F$ .<sup>16–18</sup> The  $p$ - $f$  hybridization between the pnictogen  $p$  bands and the Ce  $4f$  states plays an important role in the electronic structures near  $E_F$ . In this paper, we present the Ce  $4f$  spectra measured by the  $3d$ - $4f$  RPES for CePdX ( $X=\text{As, Sb}$ ). We compare the non- $4f$  valence-band spectra taken at the resonance-minimum ( $3d$ - $4f$ : $h\nu=875$  eV,  $4d$ - $4f$ : $h\nu=114$  eV) with the band-structure calculation of LaPdX ( $X=\text{As, Sb}$ ) (Ref. 19) and quantitatively discuss the electronic structures of the valence bands. Then we analyze the Ce  $4f$  spectra with using a noncrossing approximation (NCA) calculation<sup>20–22</sup> based on the single-impurity Anderson model (SIAM).<sup>23,24</sup> We discuss the difference between the surface and bulk electronic structures of Ce  $4f$  states for CePdX ( $X=\text{As, Sb}$ ).

## II. EXPERIMENT

The Ce  $3d$ - $4f$  RPES spectra of CePdAs were taken at the BL-2B beam line of the Photon Factory (PF) in the High Energy Accelerator Research Organization, while the  $3d$ - $4f$  RPES of CePdSb were measured at the BL-25SU beam line of SPring-8.<sup>25</sup> The Ce  $4d$ - $4f$  RPES was performed at the BL-3B (Ref. 26) beam line of the PF. These RPES spectra were taken with hemispherical GAMMADATA-SCIENZA SES-200 analyzers. The total energy resolution of the  $4d$ - $4f$  RPES ( $h\nu\sim 120$  eV) was set to about 70 meV. The total energy resolution of the  $3d$ - $4f$  RPES study of CePdAs at PF was around 0.7 eV (at  $T=300$  K), while that of CePdSb at SPring-8 was  $\sim 200$  meV at Ce  $3d$ - $4f$  threshold ( $h\nu\sim 880$  eV). The single-crystal samples of CePdX ( $X=\text{As, Sb}$ ) were prepared by the Bridgman method in evacuated tungsten-crucibles sealed by electron beam welding. The clean surfaces were obtained by repeated scraping with a diamond file *in situ* until no contamination could be detected in the photoemission region of the O  $1s$  ( $3d$ - $4f$ ) and O  $2p$  ( $4d$ - $4f$ ) signals. The base pressure was  $4\times 10^{-10}$  Torr during the measurements. For the  $3d$ - $4f$  RPES measurement for CePdSb, the sample was cooled down to 20 K by a closed-cycle He refrigerator whereas they were kept at about 40 K during the  $4d$ - $4f$  measurements. The sample temperature was kept at  $\sim 300$  K during the Ce  $3d$ - $4f$  RPES study for

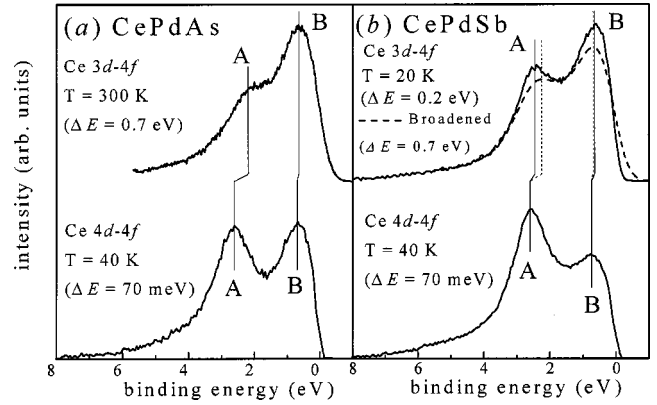


FIG. 1. Ce  $3d$ - $4f$  resonance photoemission spectra (RPES) for CePdAs (a) and CePdSb (b) compared with the  $4d$ - $4f$  RPES.

CePdAs. The binding energy ( $E_B$ ) was calibrated by the Fermi edge of Au thin film.

## III. RESULT AND DISCUSSION

Figure 1 shows the Ce  $3d$ - $4f$  RPES spectra for CePdAs (a) and CePdSb (b) in comparison with the Ce  $4d$ - $4f$  RPES spectra. The Ce  $4f$  spectra are obtained by subtracting the resonance-minimum spectra taken at  $h\nu\sim 875$  eV ( $\sim 114$  eV) from the resonance-maximum spectra taken at  $h\nu\sim 882$  eV ( $\sim 122$  eV) corresponding to the Ce  $3d$ - $4f$  ( $4d$ - $4f$ ) thresholds. Backgrounds due to the inelastic scattering are subtracted from the raw spectra in Fig. 1. The upper curve in Fig. 1(a) shows the Ce  $4f$  spectrum for CePdAs measured by means of the  $3d$ - $4f$  RPES at room temperature with the energy resolution of  $\sim 0.7$  eV. The lower curve in Fig. 1(a) for CePdAs and both upper and lower curves in Fig. 1(b) for CePdSb are measured at lower temperatures (20  $\sim$  40 K). The energy resolution of the Ce  $3d$ - $4f$  RPES for CePdSb in Fig. 1(b) is  $\sim 0.2$  eV, whereas the total energy resolution of the Ce  $4d$ - $4f$  RPES is set to 70 meV in Figs. 1(a) and 1(b). In Fig. 1(a), a two-peak structure is observed at around  $E_B=2.20$  (2.62) and 0.65 (0.70) eV in the  $3d$ - $4f$  ( $4d$ - $4f$ ) spectrum, corresponding to the anti-bonding (A) and bonding (B) states due to the hybridization between the Ce  $4f$  and other valence-band states. According to the interpretation given by the SIAM,<sup>24</sup> the peak B in the lower (smaller)  $E_B$  region derives mainly from the Ce  $4f^1$  configuration in the photoemission final states whereas the Ce  $4f^0$  final-state character is dominant in the peak A. It is found that the intensity ratio of B to A decreases remarkably from the  $3d$ - $4f$  to  $4d$ - $4f$  spectra. Since the  $4d$ - $4f$  RPES is more surface-sensitive than the  $3d$ - $4f$  RPES, the transfer of the spectral weight of the peak B to the peak A for the  $4d$ - $4f$  RPES indicates weaker hybridization strength of the Ce  $4f$  states in the surface region.

Besides, shifts of the two peaks to higher  $E_B$  are observed for the  $4d$ - $4f$  RPES. The peak B slightly shifts by  $\sim 0.05$  eV toward higher  $E_B$ . The shift of the peak A is  $\sim 0.42$  eV in CePdAs as summarized in Table I. The shift of both B [ $\Delta E(B)$ ] and A [ $\Delta E(A)$ ] peaks may originate from the localization of the bare Ce  $4f$  level due to weaker hybridization strength in the surface layer, resulting in the positive surface core-level shift. The shift of peak A includes not only

TABLE I. Summary of the experimental results on CePdAs and CePdSb. The values in the parentheses are obtained after broadening the Ce  $3d-4f$  RPES for CePdSb measured with the resolution of 0.2 eV to the resolution of 0.7 eV corresponding to the Ce  $3d-4f$  RPES of CePdAs.

Compound	$3d-4f$ RPES		$4d-4f$ RPES		Energy shift	
	$E(A)$ (broadened)	$E(B)$ (broadened)	$E(A)$	$E(B)$	$E(A)$	$E(B)$
CePdAs	2.20	0.65	2.62	0.70	0.42	0.05
CePdSb	2.45 (2.25)	0.65 (0.70)	2.60	0.75	0.15 (0.35)	0.10 (0.05)

the surface core level shift but also the so-called hybridization shift, which moves the peak  $A$  toward  $E_F$ .<sup>9</sup> Namely, the splitting between the peaks  $A$  and  $B$  increases for larger hybridization strength resulting in the shift of the peaks. According to our NCA calculation, however, the hybridization shift for the peak  $B$  is much smaller than for the peak  $A$ . Since the hybridization strength in the surface-layer is weaker than that in the bulk, the energy position of the peak  $A$  for the  $4d-4f$  RPES is shifted toward  $E_F$  for smaller hybridization effect. This contribution suggests that the surface core-level shift is larger than the observed shift  $\Delta E(A)$  as really confirmed later by NCA analysis.

Figure 1(b) shows the Ce  $3d-4f$  spectrum for CePdSb in comparison with the  $4d-4f$  RPES spectrum. There are two-peak features at around 2.45 (2.60) and 0.65 (0.75) eV in the  $3d-4f$  ( $4d-4f$ ) RPES results. Similarly to CePdAs, the intensity ratio of  $B$  to  $A$  reduces much in the  $4d-4f$  RPES and the energy positions of the peak  $B$  and  $A$  shift toward higher  $E_B$ . However, the energy shift of the peak  $B$  ( $A$ ) is  $\sim 0.10$  (0.15) eV, which is larger (smaller) than the corresponding value of CePdAs as summarized in Table I. In order to properly compare this value with the result of CePdAs, the  $3d-4f$  RPES result for CePdSb is convoluted with a Gaussian function to achieve the same energy resolution ( $\sim 0.7$  eV). After this broadening process, we notice that the energy separation of the two peaks is smaller (1.80 $\rightarrow$ 1.55 eV) and the energy shift  $\Delta E(B)$  and  $\Delta E(A)$  become comparable to those of CePdAs, namely 0.35 and 0.05 eV compared with 0.42 and 0.05 eV. In other words, better resolution measurements for CePdAs may lead to larger (smaller) energy shift of  $\Delta E(B)$  [ $\Delta E(A)$ ] than the value in Table I and the intensity of the peak  $B$  may be more enhanced. The intensity ratio of  $B$  to  $A$  is larger for CePdAs than for CePdSb, showing that the hybridization strength is stronger for CePdAs. The change of the hybridization strength is due to the difference of the pnictogen and/or the crystal structures.

Figure 2(a) compares the  $3d-4f$  resonance-minimum spectra between CePdAs (empty circle) and CePdSb (solid curve). All spectra are normalized to the same area after the subtraction of the inelastic electron background. The spectrum for CePdSb is broadened with a 0.7 eV full width at half maximum (FWHM) Gaussian function by considering the different resolution. The resonance-minimum spectra taken at  $h\nu \sim 875$  eV have rather similar spectral line shape, namely they have a prominent peak structure at around 3.3 eV, a shoulder structure at around 1.3 eV, and a linearly decreasing feature toward  $E_F$ , in spite of the difference of

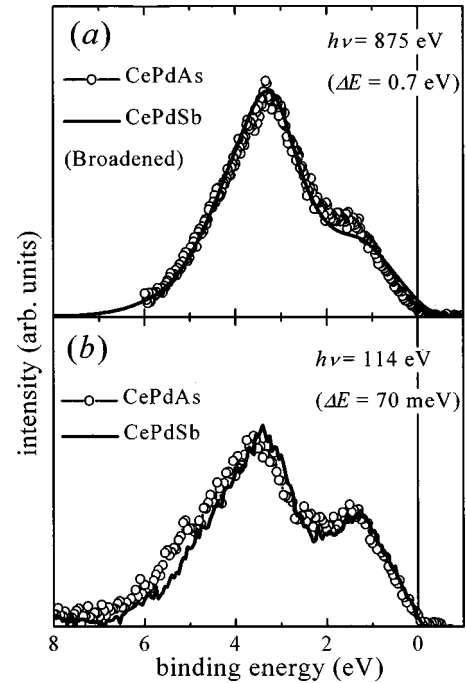


FIG. 2. Comparison of the resonance-minimum spectra of CePdAs (empty circle) and CePdSb (solid curve) taken at  $h\nu = 875$  (a) and 114 eV (b). The spectrum of CePdSb taken at  $h\nu = 875$  eV is broadened to the energy resolution ( $\Delta E = 0.7$  eV) of the spectrum of CePdAs.

pnictogen. The similarity of the spectra between two compounds should be ascribed to the large photoionization cross section of the Pd  $4d$  states in this excitation energy region.<sup>27</sup> Figure 2(b) shows the resonance-minimum spectra taken at  $h\nu \sim 114$  eV for reference. Both spectra for CePdAs and CePdSb have common features in regard to the peak structures at 3.3 and 1.3 eV along with the tendency of decrease toward  $E_F$ . One notices for both compounds that the intensity of the prominent peak near 3.3 eV with respect to the intensity of the 1.3 eV structure is noticeably weaker than the  $3d-4f$  resonance-minimum spectra. This is because the photon energy ( $h\nu \sim 114$  eV) corresponds to the Cooper minimum for the Pd  $4d$  states.<sup>27</sup>

In order to understand the valence-band structures of both CePdAs and CePdSb, we will compare the results of the band-structure calculations for isostructural La compounds LaPdAs and LaPdSb performed by a full-potential linear augmented plane wave method.<sup>19,28</sup> Comparison of the total density of states (DOS) between LaPdAs and LaPdSb is shown in the upper panel of Fig. 3, while the lower panel of Fig. 3 displays the partial DOS (PDOS) for each element, namely La  $5d$ , Pd  $4d$ , and pnictogen  $p$  orbits for both compounds. The results for both compounds are rather similar. The total DOS for both compounds is decreasing toward  $E_F$  and extremely small at  $E_F$  as experimentally observed. This indicates that these compounds belong to the low-carrier system. Judging from the PDOS for dominant orbits, the Pd  $4d$  states are dominant for the total DOS in wide valence-band region below  $E_F$ , in particular, in the region from  $\sim 2.5$  to  $\sim 3.7$  eV. This may be derived from a nonbonding Pd  $4d$  states. The As  $4p$  and Sb  $5p$  states below  $E_F$  have noticeable PDOS in the two regions from  $\sim 3.6$  to  $\sim 5.5$  eV and from

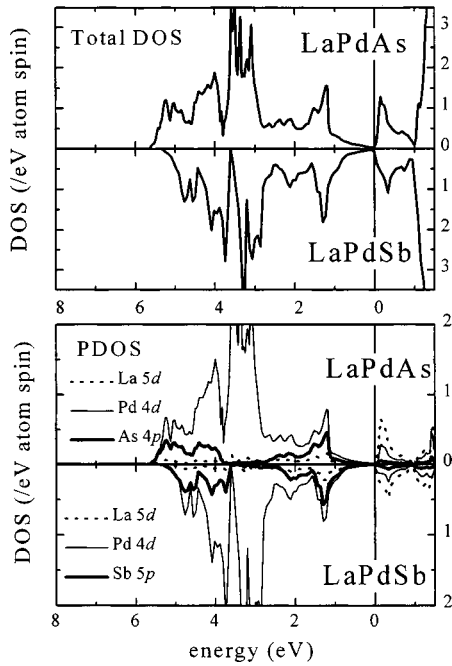


FIG. 3. Comparison of the density of states (DOS) obtained by the band-structure calculation for LaPdAs and LaPdSb (Ref. 19). The partial DOS (PDOS) of the La 5*d*, Pd 4*d*, and As 4*p* (Sb 5*p*) states in LaPdAs (LaPdSb) are shown in the lower panel.

$\sim 2.5$  to  $0.5$  eV. The former region may correspond to the bonding states between the Pd 4*d* and pnictogen *p* states while the latter region corresponds to their antibonding states. The structures ranging from  $5.5$  to  $2.5$  eV, namely the bonding states between the Pd 4*d* and pnictogen *p* states and the Pd 4*d* nonbonding states, shift to lower  $E_B$  from LaPdAs to LaPdSb. This may arise from the shift of the pnictogen *p*-band states toward  $E_F$  by the substitution of As by Sb.

In order to more quantitatively discuss the electronic structure of the valence bands, we compare a valence-band spectrum of CePdSb, which is obtained by Ce 3*d*-4*f* resonance-minimum spectrum ( $h\nu \sim 875$  eV), with the PDOS obtained by the band-structure calculation for LaPdSb in Fig. 4(a).<sup>19</sup> The experimental non-4*f* valence-band spectrum consists of a main peak at  $\sim 3.3$  eV, a shoulder structure at  $\sim 4.0$  eV and a broad structure at  $\sim 1.3$  eV. In order to simplify a comparison between experimental and calculated results (shown in the lower panel of Fig. 3), we tentatively convolute the calculated PDOS results with use of both Lorentzian broadening with the maximum FWHM of  $0.5$  eV (Ref. 29) and Gaussian broadening with a fixed FWHM of  $0.2$  eV corresponding to the instrumental resolution ( $\Delta E \sim 0.2$  eV). The Lorentzian width originates from a lifetime of the photoemission final states. In addition, we take the photoionization cross section at this excitation energy into account.<sup>27</sup> We summarized the convoluted PDOS in the bottom of Fig. 4(a). The Pd 4*d* contribution is much stronger than others ( $\sigma_{\text{Pd}4d}/\sigma_{\text{Sb}5p} \sim 20$  and  $\sigma_{\text{Pd}4d}/\sigma_{\text{La}5d} \sim 30$ ).<sup>27</sup> The thick-solid curve obtained by adding all PDOS components well reproduces the experimental spectrum. The main peak at around  $3.3$  eV, a shoulder at around  $4$  eV, and a broad structure at around  $1.3$  eV are well reproduced. Thus, it is found that the 3*d*-4*f* resonance-minimum spectrum is almost composed of the Pd 4*d* states. Although the weight of

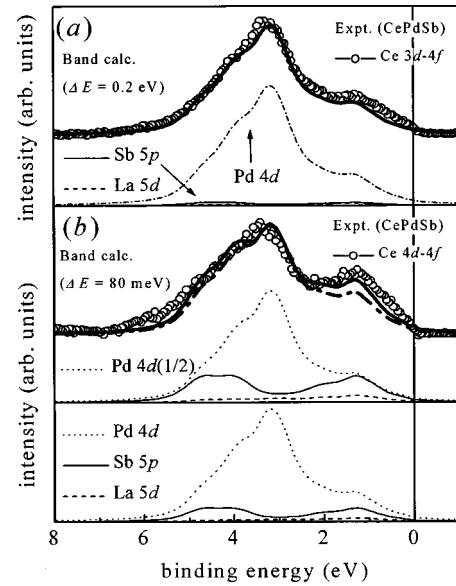


FIG. 4. Resonance-minimum spectrum of CePdSb taken at the Ce 3*d* (a) and 4*d* (b) thresholds compared with the results of the band-structure calculation. The PDOS broadened by a Gaussian and a Lorentzian function in LaPdSb are also displayed, considering the relative photoionization cross sections. See text for details.

the Sb 5*p* and La 5*d* states is small, they contribute to such spectral structures as the shoulder at around  $4$  eV and the peak near  $1.3$  eV through the hybridization with the Pd 4*d* states. Some difference between the calculated DOS and experimental spectrum, for example near  $1$  eV, may arise from the ignorance of the final-state hybridization of the valence bands with the Ce 4*f* states.

For reference, Fig. 4(b) displays the PDOS of LaPdSb in the bottom panel and the relatively surface-sensitive valence-band spectrum for CePdSb taken at  $h\nu \sim 114$  eV in the upper panel. This excitation photon energy corresponds to the Cooper minimum of the Pd 4*d* states, thus the relative ratios of the photoionization cross sections reduce as  $\sigma_{\text{Pd}4d}/\sigma_{\text{Sb}5p} \sim 4$  and  $\sigma_{\text{Pd}4d}/\sigma_{\text{La}5d} \sim 20$ .<sup>27</sup> The PDOS in Fig. 4(b) are obtained by the above-mentioned broadening process. In the upper panel of Fig. 4(b) is shown the sum of PDOS by the dot-dashed curve with using the reported cross section parameters in Ref. 27. However, one notices a remarkable discrepancy near  $\sim 1.3$  eV. The result suggests a possibility of further suppression of  $\sigma_{\text{Pd}4d}$  in the Cooper minimum region. We try to reproduce the experimental result by reducing the relative intensities by half. The thick solid curve in the upper panel of Fig. 4(b) shows the sum of three components. The shoulder structure near  $1.3$  eV is better explained. Thus, we confirm that the band-structure calculation well reproduces the experimental results of the valence bands. The difference between the 3*d*-4*f* and 4*d*-4*f* spectra can be explained by the  $h\nu$  dependence of the photoionization cross sections. Hence, no surface effect is detected in the electronic structure of the valence-band spectra.

In order to discuss the difference of the Ce 4*f* electronic structures between CePdAs and CePdSb as well as between bulk and surface, we calculate the Ce 4*f* spectra by the NCA method within SIAM. The  $I_s/I_b$  is given by  $\exp(d/\lambda) - 1$ , where  $d$  is the thickness of the surface layer and  $\lambda$  is the photoelectron mean-free path as a function of the kinetic

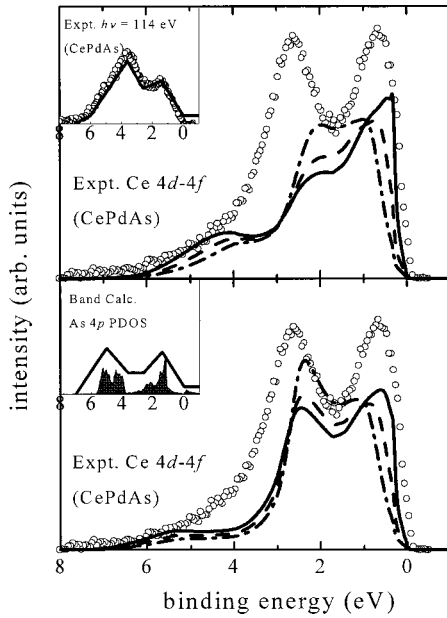


FIG. 5. Hybridization strength  $\rho V^2(E)$  dependence of the NCA spectra compared with the  $4d-4f$  resonance photoemission spectra of CePdAs. The upper inset shows the energy dependence of the hybridization strength employed for the NCA calculation shown in the upper panel, which corresponds to the  $4d-4f$  resonance-minimum spectrum of CePdAs. The lower inset compares the PDOS of As  $4p$  states with the energy distribution  $\rho V^2(E)$  employed for the NCA spectra shown in the lower panel.

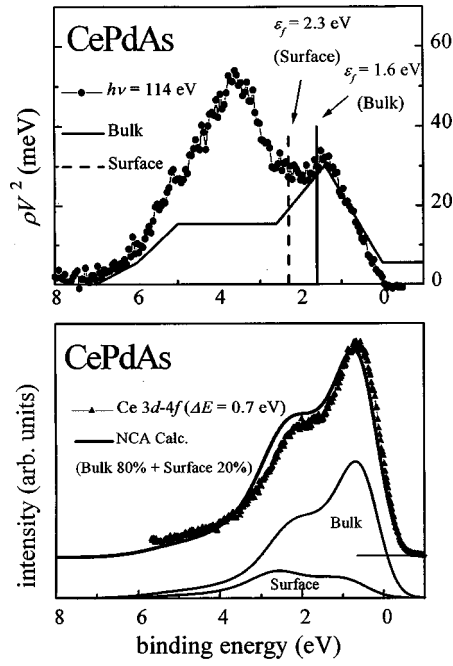
energy ( $\lambda$  is about 4 and 15 Å at the Ce  $4d$  and Ce  $3d$  thresholds, respectively).<sup>30</sup> The value of  $d$  is assumed to be 3.9 Å for both compounds (the nearest neighbor Ce-Ce distance is 3.899 and 3.947 Å for CePdAs and CePdSb, respectively).<sup>13,31</sup> We obtain  $I_s/I_b \sim 1.63$  and 0.25 for Ce  $4d-4f$  and Ce  $3d-4f$  RPES, respectively. We tried to divide the observed Ce  $4f$  spectrum into the surface and bulk components in a direct way without employing the simple subtraction method, which has been widely used in separating the spectrum into the surface and bulk contributions.<sup>5-10</sup> Namely we fit the experimental results by a sum of surface and bulk components with the given surface/bulk intensity ratio. The energy dependence of the hybridization strength  $\rho V^2(E)$  to reproduce the experimental results is first assumed to be proportional to the resonance-minimum spectrum, which has two-peak structures at 3.6 and 1.4 eV as shown in the upper inset of Fig. 5. The upper panel shows the hybridization strength dependence of the Ce  $4f$  spectrum for CePdAs.  $\rho V^2(E)$  was simulated by the energy dependence shown in the upper inset. The solid, dashed, and dot-dashed curves in the upper panel correspond to  $\rho V^2(E_F) = 5.0, 4.0,$  and  $3.0$  meV. The bulk and surface components are added in the calculated curves with the intensity ratio of  $I_s/I_b \sim 1.63$ . We set the bare  $4f$  level ( $\epsilon_f$ ) for the surface and bulk states to 2.3 and 1.6 eV, respectively. Although the hybridization strength is varied in the whole energy range, the experimental spectrum cannot be well reproduced. The strong hybridization near 3.6 eV with the Pd  $4d$  states splits the  $4f$  component into higher and lower  $E_B$  components. The noticeable discrepancy suggests that the resonance-minimum spectrum does not faithfully reflect the energy dependence of the hybridization strength with the Ce  $4f$  states.

This result suggests that the  $p-f$  mixing can be stronger than the  $d-f$  mixing for these Ce pnictide compounds.

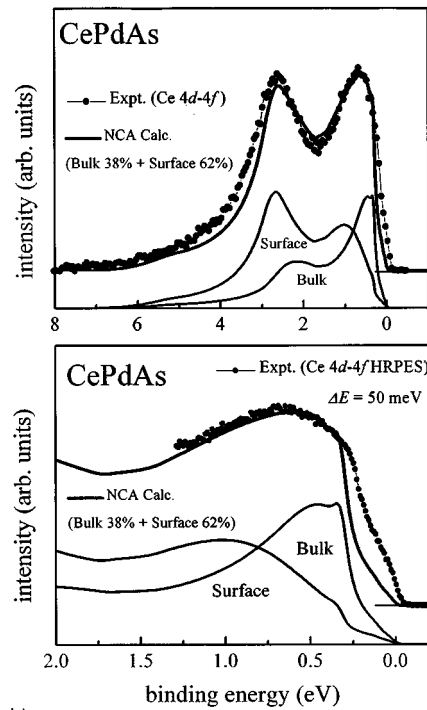
Then, we attempted to calculate the Ce  $4f$  spectra by considering the hybridization strength  $\rho V^2(E)$  represented by the pnictogen  $p$ -band-like energy dependence of DOS, which has the two-peak structures near 5.0 and 1.6 eV as shown in the lower inset of Fig. 5. The hybridization strength dependence of the Ce  $4f$  spectrum in the entire valence-band region is shown in the lower panel of Fig. 5. The experimental  $4f$  spectrum of CePdAs is compared with the calculated curves, which are obtained by the sum of the surface ( $\epsilon_f = 2.3$  eV) and bulk (1.6 eV) components with the ratio of  $I_s/I_b \sim 1.63$ . Although the calculated  $4f$  spectra have two-peak structures, the spectral weights from 3 to 5 eV are much suppressed and deviated from the experimental Ce  $4f$  spectrum. The discrepancy is ascribed to the strong hybridization strength near 5.0 eV, indicating that the simple assumption that  $\rho V^2(E)$  is represented by the PDOS of the pnictogen  $p$  states is improper. Then, we assume that  $\rho V^2(E)$  has one peak near 1.3 eV corresponding to the antibonding states between the Pd  $4d$  and pnictogen  $p$  states. Such an energy dependence as shown in the upper panel of Fig. 6(a) better reproduces the two-peak structures of the Ce  $4f$  spectra displayed in Fig. 1 as later shown in the lower panel of Fig. 6(a). Thus, the Ce  $4f$  states may be strongly hybridized with the antibonding states of the  $p-d$  mixed states.

In order to discuss the difference between the surface and bulk electronic structures for the two compounds, we have performed the NCA calculation for the bulk- and surface-sensitive Ce  $4f$  spectra. The solid line in the upper panel of Fig. 6(a) shows the energy distribution  $\rho V^2(E)$  used for the calculation in comparison with the resonance-minimum spectrum (dots) for CePdAs taken at  $h\nu = 114$  eV. This  $\rho V^2(E)$  emphasizes the strong hybridization of the Ce  $4f$  states with the anti-bonding states between the Pd  $4d$  and As  $4p$  states at around 1.4 eV. The  $\rho V^2(E)$  linearly decreases toward  $E_F$  and is assumed to be constant above  $E_F$  with  $\rho V^2(E_F) = 5.5$  meV. The remaining DOS above  $E_F$  represents the finite DOS of the conduction-band states as shown in Fig. 3. We set the  $\epsilon_f$  to 1.6 and 2.3 eV for the bulk and surface, respectively. Here, the spin-orbit splitting of the Ce  $4f$  states of 0.32 eV is used. The calculated curve, which is a sum of the surface and bulk components with the ratio of  $I_s/I_b \sim 0.25$ , well reproduces the bulk-sensitive  $3d-4f$  RPES spectrum for CePdAs in the lower panel of Fig. 6(a). It is noticed that the bulk contribution is dominant in the whole region. The surface-sensitive  $4d-4f$  spectrum measured with the energy resolution of  $\Delta E \sim 70$  meV is qualitatively reproduced by the sum of surface and bulk spectra with the intensity ratio of  $I_s/I_b \sim 1.63$  in the upper panel of Fig. 6(b). The calculated result is compared with the RPES spectrum ( $\Delta E \sim 50$  meV) in the vicinity of  $E_F$  in the lower panel of Fig. 6(b). The same calculation also qualitatively reproduces the experimental line shape in this energy region, in particular the weak shoulder structures at  $\sim 0.25$  and  $\sim 0.05$  eV. It is recognized that the surface electronic states give strong influence on the Ce  $4f$  spectrum measured by the  $4d-4f$  RPES up to  $E_F$ . The surface effect is mostly treated by the shift of the bare Ce  $4f$  level.

Similar results for CePdSb are shown in the upper panel



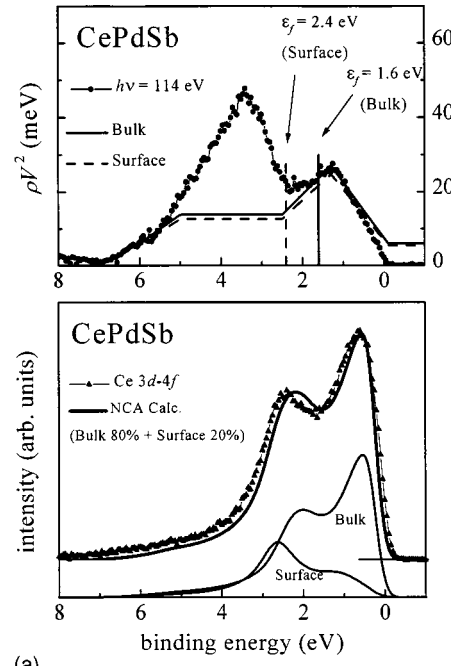
(a)



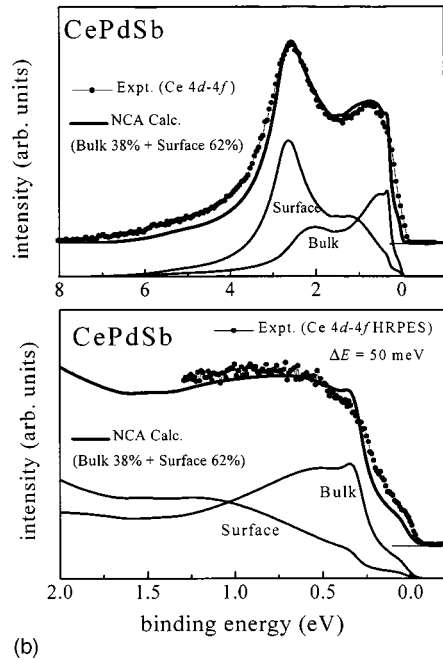
(b)

FIG. 6. (a) Upper panel: Comparison of the optimized energy dependence of the hybridization strength and parameters used in the NCA calculation with the  $4d-4f$  resonance-minimum spectrum of CePdAs. Lower panel: Comparison of the Ce  $4f$  spectrum studied by the  $3d-4f$  RPEs with the calculated spectrum for CePdAs in the wide-energy region. (b) Comparison of the calculated results with the Ce  $4f$  component measured by the  $4d-4f$  RPEs in the wide region (upper panel) and near  $E_F$  (lower panel).

of Fig. 7(a). The  $\rho V^2(E)$  represents the strong hybridization of the Ce  $4f$  states with the antibonding states between the Pd  $4d$  and Sb  $5p$  states centered at 1.3 eV. The  $\rho V^2(E)$  decreases toward  $E_F$ , and the DOS just above  $E_F$  is assumed to be  $\rho V^2(E)$  is 6.0 and 5.5 meV for bulk and surface, re-



(a)



(b)

FIG. 7. Comparison for CePdSb. (a) The optimized energy distribution  $\rho V^2(E)$  for bulk (solid line) and surface (broken line) components. The lower panel shows the  $4f$  spectrum obtained from the Ce  $3d-4f$  RPEs compared with the NCA calculation. (b) Comparison of the  $4f$  spectrum measured by the Ce  $4d-4f$  spectrum in the wide-energy region (upper panel) and near  $E_F$  (lower panel) with the NCA calculation.

spectively. The  $\epsilon_f = 1.6(2.4)$  eV is employed for the bulk (surface). The calculated result with  $I_s/I_b = 0.25$  can well explain the bulk-sensitive  $3d-4f$  RPEs spectrum measured with the energy resolution of  $\Delta E \sim 200$  meV as shown in the lower panel of Fig. 7(a). The surface-sensitive  $4d-4f$  spectrum is properly reproduced by the calculated curve with  $I_s/I_b = 1.63$  in the upper panel of Fig. 7(b). The lower panel displays the experimental  $4f$  spectrum near  $E_F$ . In this re-

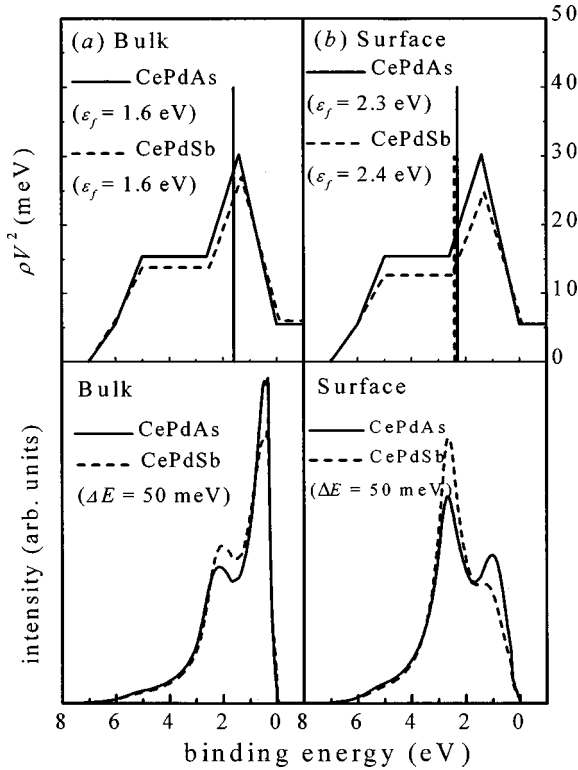


FIG. 8. Summary of the energy dependence of the hybridization strength  $\rho V^2(E)$  employed for the optimized NCA calculations. The bare  $4f$  level energy  $\epsilon_f$  is also shown in the upper figure. The calculated bulk and surface spectra are shown for CePdX ( $X = \text{As, Sb}$ ) in the lower panel.

gion, the calculated  $4f$  spectrum also agrees qualitatively with the experimental result. Here again, the surface effect is mainly described by the shift of the bare  $4f$  level. These results support the validity of the SIAM to explain the present Ce  $4f$  spectra. Generally speaking, the Ce  $4d$ - $4f$  RPES spectra deviate obviously from the bulk electronic structures due to the remarkable contribution from the surface layer while the Ce  $3d$ - $4f$  RPES spectra are dominated by the bulk component.

We summarize the  $\rho V^2(E)$  used in the reproduction of the Ce  $4f$  spectra for CePdAs and CePdSb in the upper panel of Fig. 8. The panel (a) represents the bulk component and (b) represents the surface component. The bulk  $\epsilon_f$  is 1.6 eV for both CePdAs and CePdSb, whereas surface  $\epsilon_f$  is 2.3 eV for CePdAs and 2.4 eV for CePdSb. The lower panels of Fig. 8 show the spectra calculated by NCA method. An important issue from this analysis is that the employed  $\rho V^2(E)$  in reproducing the Ce  $4f$  spectra has not directly reflected the resonance-minimum spectra or the pnictogen  $p$  states. It suggests that a profound investigation of the hybridization mechanism is needed to analyze the Ce  $4f$  photoemission spectra. The average hybridization strength  $\Delta = \pi \int_0^B \rho V^2(E) dE / B$  for bulk components of CePdAs ( $\Delta = 46.0$  meV) is stronger than that for CePdSb ( $\Delta = 42.3$  meV). The calculated bulk spectra for the two compounds in the lower panel of Fig. 8(a) reveal that the change of the average hybridization strength  $\Delta$  leads to the difference in the intensity ratio of the two peaks.

The  $\rho V^2(E)$  for the surface component is shown in the upper panel of Fig. 8(b). Here, the average hybridization strength  $\Delta$  is taken as 46.0 and 38.8 meV for CePdAs and CePdSb, respectively. The lower panel of Fig. 8(b) compares the surface spectrum for both compounds. Although the difference between the surface and bulk electronic structures is almost explained by considering the shift of the bare  $4f$  level, the difference of the Ce  $4f$  spectra between these two compounds are mainly attributed to the difference of the hybridization strength  $\rho V^2(E)$ . The  $4f$  electron number ( $n_f$ ) of CePdAs is estimated as  $\sim 0.994$  (0.996) for the bulk (surface), while the  $n_f$  of CePdSb is  $\sim 0.994$  (0.997) for the bulk (surface) component. These results are consistent with weakly hybridized feature of both compounds.

#### IV. CONCLUSION

In conclusion, we have performed  $3d$ - $4f$  RPES for weakly hybridized Ce compounds, CePdAs and CePdSb. The Ce  $4f$  spectra of the two compounds have two-peak structures corresponding to the  $4f^1$  and  $4f^0$  final-states but their intensity ratios are rather different. The spectral difference is interpreted as due to the difference of the hybridization of the Ce  $4f$  states with other valence bands. The bulk-sensitive  $3d$ - $4f$  RPES spectra for both compounds show stronger hybridization feature than those of the surface-sensitive  $4d$ - $4f$  RPES, revealing the essential difference between the surface and bulk electronic structures. On the other hand, the resonance-minimum spectra are rather similar between the two compounds. The results were compared with the band-structure calculations for LaPdAs and LaPdSb. The resonance-minimum spectra for CePdSb are compared with the calculated results by taking the photoionization cross sections and the instrumental resolution into account. It is shown that the surface effect is negligible in the resonance-minimum spectra or the valence-band spectra. However, the NCA calculation has revealed that  $\rho V^2(E)$  reflected in the resonance-minimum spectra cannot satisfactorily reproduce the experimental Ce  $4f$  spectra. We can reproduce the surface- and bulk-sensitive Ce  $4f$  spectra of both compounds and separate the surface and bulk components by considering the  $\rho V^2(E)$  associated with the antibonding states of the  $p$ - $d$  mixed states. The difference between the surface and bulk electronic states can be treated by considering the surface core level shift of the bare  $4f$  level, while the difference between the two compounds is mainly described by the different energy dependence of the hybridization strength. The Ce  $3d$ - $4f$  spectra semiquantitatively reflect the bulk component, supporting that the high energy excitation RPES is a powerful means to probe bulk electronic structures. We have reconfirmed the validity of the SIAM to explain the Ce  $4f$  photoemission spectra, at least for weakly hybridized (low  $T_K$ ) Ce compounds.

#### ACKNOWLEDGMENTS

We would like to thank the staffs of PF, especially M. Mamiya, A. Kakizaki, Y. Azuma, and E. Shigemasa, and the staffs of SPring-8 for supporting the experiment. We thank K. V. Kaznacheyev, T. Susaki, T. Shishidou, T.

Kimura, T. Yasuda, and R.-J. Jung for their technical support. The authors are much obliged to A. Yagishita, T. Miyahara, and A. Fujimori for their fruitful advice. This work was supported by a Grant-in-Aid for COE Research (10CE2004) of the Ministry of Education, Science, Sports, and Culture,

Japan. The measurements were performed at PF under the approval of the Photon Factory Program Advisory Committee (92S002) and the studies at SPring-8 were performed with the approval of the Japan Synchrotron Radiation Research Institute (JASRI) (Proposal No. 1997B1043-NS-np).

- 
- \*Present address: Photon Factory, KEK, Tsukuba, Ibaragi 305-0801, Japan.
- <sup>†</sup>Present address: Japan Synchrotron Radiation Research Institute, SPring-8, Mikazuki, Hyogo 679-5198, Japan.
- <sup>‡</sup>Present address: ERATO, JST, KSP, Takatsu, Kawasaki, Kanagawa, 213-0012, Japan.
- <sup>1</sup>J.C. Fuggle, F.U. Hillebrecht, Z. Zolnierok, R. Lässer, Ch. Freiburg, O. Gunnarsson, and K. Schönhammer, *Phys. Rev. B* **27**, 7330 (1983).
- <sup>2</sup>J.W. Allen, S.-J. Oh, O. Gunnarsson, K. Schönhammer, M.B. Maple, M.S. Torikachvili, and I. Lindau, *Adv. Phys.* **35**, 275 (1986).
- <sup>3</sup>A. Kakizaki, A. Harasawa, T. Ishii, T. Kashiwakura, A. Kamata, and S. Kunii, *J. Phys. Soc. Jpn.* **64**, 302 (1995).
- <sup>4</sup>M. Tsunekawa, S. Suga, A. Kimura, T. Matsushita, T. Muro, S. Ueda, H. Daimon, S. Imada, T. Nakatani, Y. Saitoh, T. Iwasaki, A. Sekiyama, A. Fujimori, H. Ishii, T. Miyahara, T. Hanyu, H. Namatame, M. Taniguchi, E. Shigemasa, O. Sakai, R. Takayama, R. Settai, H. Azuma, and Y. Onuki, *Solid State Commun.* **103**, 659 (1997).
- <sup>5</sup>C. Laubschat, E. Weschke, C. Holtz, M. Domke, O. Strebels, and G. Kaindl, *Phys. Rev. Lett.* **65**, 1639 (1990).
- <sup>6</sup>E. Weschke, C. Laubschat, T. Simmons, M. Domke, O. Strebels, and G. Kaindl, *Phys. Rev. B* **44**, 8304 (1991).
- <sup>7</sup>C. Laubschat, E. Weschke, M. Domke, C.T. Simmons, and G. Kaindl, *Surf. Sci.* **269/270**, 605 (1992).
- <sup>8</sup>G. Chiaia, P. Vavassori, L. Duò, L. Braicovich, M. Qvarford, and I. Lindau, *Surf. Sci.* **331-333**, 1229 (1995).
- <sup>9</sup>L. Duò, *Surf. Sci.* **377-379**, 160 (1997).
- <sup>10</sup>H.-D. Kim, O. Tjernberg, G. Chiaia, H. Kumigashira, T. Takahashi, L. Duò, O. Sakai, M. Kasaya, and I. Lindau, *Phys. Rev. B* **56**, 1620 (1997).
- <sup>11</sup>A. Sekiyama, S. Suga, Y. Saitoh, S. Ueda, H. Harada, T. Matsushita, T. Nakatani, T. Iwasaki, K. Matsuda, M. Kotsugi, S. Imada, T. Takabatake, T. Yoshino, D.T. Adroja, R. Takayama, O. Sakai, H. Harima, and T. Nanba, *Solid State Commun.* **111**, 373 (1999).
- <sup>12</sup>K. Katoh, A. Ochiai, and T. Suzuki, *Physica D* **223&224**, 340 (1996).
- <sup>13</sup>S.K. Malik and D.T. Adroja, *Phys. Rev. B* **43**, 6295 (1991).
- <sup>14</sup>B.D. Rainford, D.T. Adroja, A. Neville, and D. Fort, *Physica B* **206&207**, 209 (1995).
- <sup>15</sup>T. Iwasaki, S. Suga, S. Imada, Y. Kuwata, T. Muro, S. Ueda, M. Saeki, H. Harada, M. Tsunekawa, T. Matsushita, A. Sekiyama, A. Fujimori, H. Ishii, T. Kimura, T. Miyahara, T. Suzuki, K. Katoh, and A. Ochiai, *J. Electron Spectrosc. Relat. Phenom.* **88-91**, 309 (1998).
- <sup>16</sup>H. Kumigashira, S.-H. Yang, T. Yokoya, A. Chainani, T. Takahashi, A. Uesawa, and T. Suzuki, *Phys. Rev. B* **55**, 3355 (1997).
- <sup>17</sup>A. Franciosi, J.H. Weaver, N. Mårtensson, and M. Croft, *Phys. Rev. B* **24**, 3651 (1981).
- <sup>18</sup>A. Fujimori, M. Grioni, J.J. Joyce, and J.H. Weaver, *Phys. Rev. B* **31**, 8291 (1985).
- <sup>19</sup>M. Akuura, and T. Oguchi (unpublished).
- <sup>20</sup>N.E. Bickers, D.L. Cox, and J.W. Wilkins, *Phys. Rev. B* **36**, 2036 (1987).
- <sup>21</sup>N.E. Bickers, *Rev. Mod. Phys.* **59**, 846 (1987).
- <sup>22</sup>Y. Kuramoto, *Z. Phys.* **53**, 37 (1983).
- <sup>23</sup>P.W. Anderson, *Phys. Rev.* **124**, 41 (1961).
- <sup>24</sup>O. Gunnarsson and K. Schönhammer, in *Handbook on the Physics and Chemistry of Rare Earths*, edited by K. A. Gschneidner, L. Eyring, and S. Hüfner (Elsevier, Amsterdam, 1987), Vol. 10, pp. 103–163.
- <sup>25</sup>Y. Saitoh, T. Nakatani, T. Matsushita, T. Miyahara, M. Fujisawa, K. Soda, T. Muro, S. Ueda, H. Harada, A. Sekiyama, S. Imada, H. Daimon, and S. Suga, *J. Synchrotron Radiat.* **5**, 542 (1998).
- <sup>26</sup>A. Yagishita, T. Hayaishi, T. Kikuchi, and E. Shigemasa, *Nucl. Instrum. Methods Phys. Res. A* **306**, 578 (1991).
- <sup>27</sup>J.J. Yeh, and I. Lindau, *At. Data Nucl. Data Tables* **32**, 1 (1985).
- <sup>28</sup>E. Wimmer, H. Krakauer, M. Weinert, and A.J. Freeman, *Phys. Rev. B* **24**, 864 (1981).
- <sup>29</sup>At each  $E_B$ , a Lorentzian contribution is considered, whose FWHM is assumed to increase with  $E_B$  reflecting the shorter lifetime.
- <sup>30</sup>S. Tanuma, C.J. Powell, and D.R. Penn, *Surf. Sci.* **192**, L849 (1987).
- <sup>31</sup>D. Johrendt, A. Mewis, *J. Alloys Compd.* **183**, 210 (1992).